Lawrence Berkeley Laboratory
UNIVERSITY OF CALIFORNIA
Physics Division

Invited talk presented at the Symposium on High Energy e^+e^- Interactions, Vanderbilt University, Nashville, TN, April 5-7, 1984

HADRON PRODUCTION IN e^+e^- ANNIHILATION AT PEP

W. Hofmann

May 1984

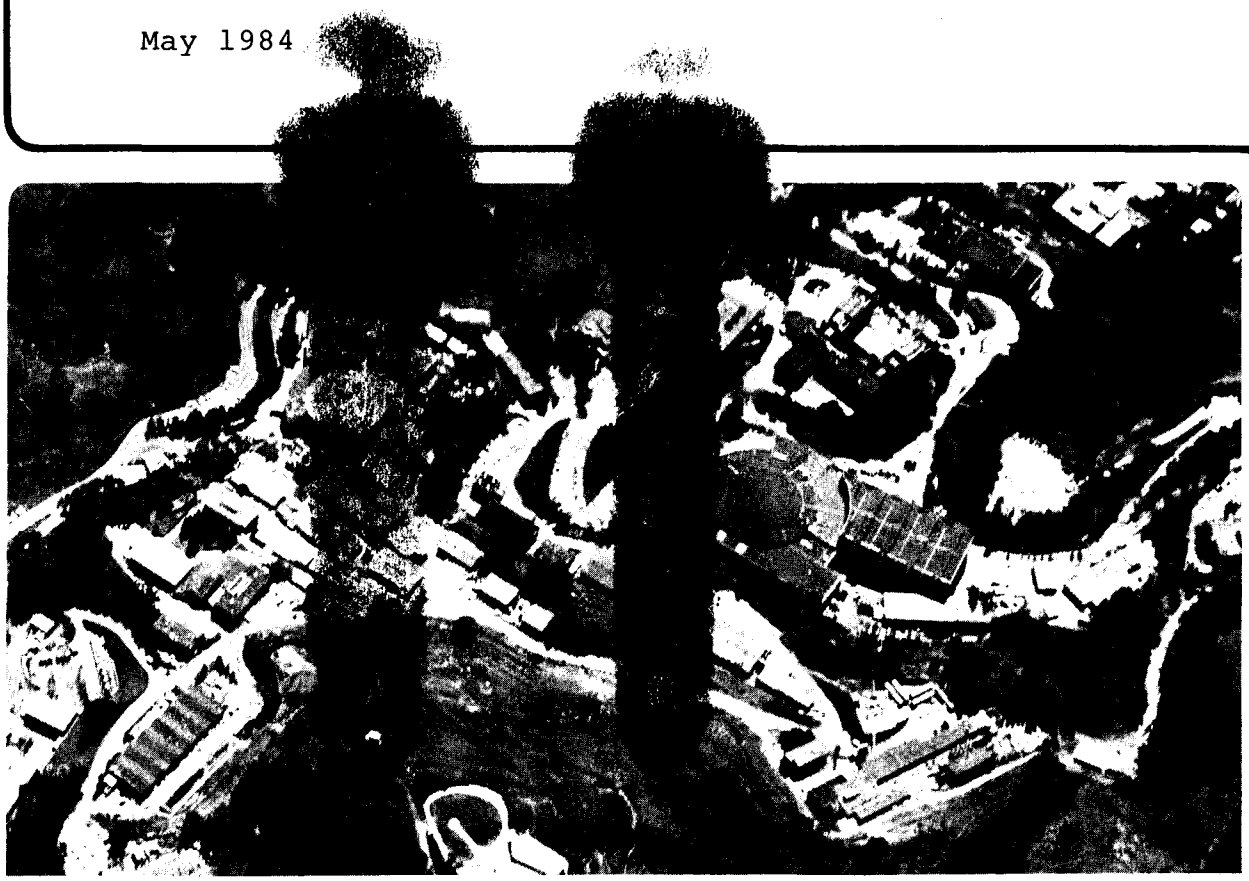

Prepared for the U.S. Department of Energy under Contract DE-AC03-76SF00098

DISCLAIMER

LBL-17845

Hadron Production in e^+e^- Annihilation at PEP

Werner Hofmann

Lawrence Berkeley Laboratory, University of California

Berkeley, California 94720

May 1984

ABSTRACT: Recent results from PEP on quark and gluon fragmentation are reviewed. Topics include: inclusive stable particle production and resonance production, particle distributions in jets, heavy quark fragmentation, flavor correlation studies and tests of fragmentation models.

Invited Talk presented at the

Symposium on High Energy e^+e^- Interactions

Vanderbilt University, Nashville, Tennessee

April 5-7, 1984

Hadron Production in e^+e^- Annihilation at PEP

Werner Hofmann

Lawrence Berkeley Laboratory, University of California
Berkeley, California 94720

Our present picture of the process of hadron production in e^+e^- annihilation is outlined in fig. 1. A virtual photon creates the initial $q\bar{q}$ pair. At early times, these quarks are far off-shell and propagate according to perturbative QCD, emitting radiative gluons. In the next stage of hadronization new $q\bar{q}$ pairs materialize. Quarks and antiquarks then combine to form colorless hadronic systems (resonances or "clusters").

Two extreme models for this crucial step responsible for color confinement are the "string" picture [1] and parton shower models based on QCD [2-5]. The string model assumes the formation of an entirely nonperturbative, one-dimensional color force field between the initial quarks. This force field is discharged by production of $q\bar{q}$ pairs screening the field. In parton shower models, the initial quark cascades down to its mass-shell by successive gluon emission; the gluons in turn emit further gluons or convert into $q\bar{q}$ pairs, creating a parton shower. The parton "decay" is governed by the familiar Altarelli-Parisi equations [6]. The main difference between the two pictures is the Q^2 scale where nonperturbative effects take over: in the string model the perturbative evolution is cut off at large $Q^2 \approx 10\text{-}100$ GeV^2, whereas shower models use QCD down to $Q^2 \approx 1$ GeV^2.

In a final step, the color singlets formed in the confinement phase will decay to the stable hadrons ultimately observed in the detectors. Since each step requires a certain average proper time, the boundaries between the areas indicated in fig. 1 form hyperbolas in space-time. The result is an inside-out cascade [7], where the slowest hadrons are produced first.

The major problem in extracting the dynamics of quark fragmentation from the data is evident from fig. 1: the most interesting regions of confinement and perturbative QCD are veiled by the effects of resonance (or cluster) decays; the QCD phase is furthermore obscured by the confinement process.

This paper is structured in analogy to fig. 1. We will proceed in the direction of increasing complexity: first, stable particle production will be discussed. Next, we consider effects involving more than one final state particle: resonance production and properties of jets and of particles in a jet environment. The study of heavy quark fragmentation and of flavor correlations

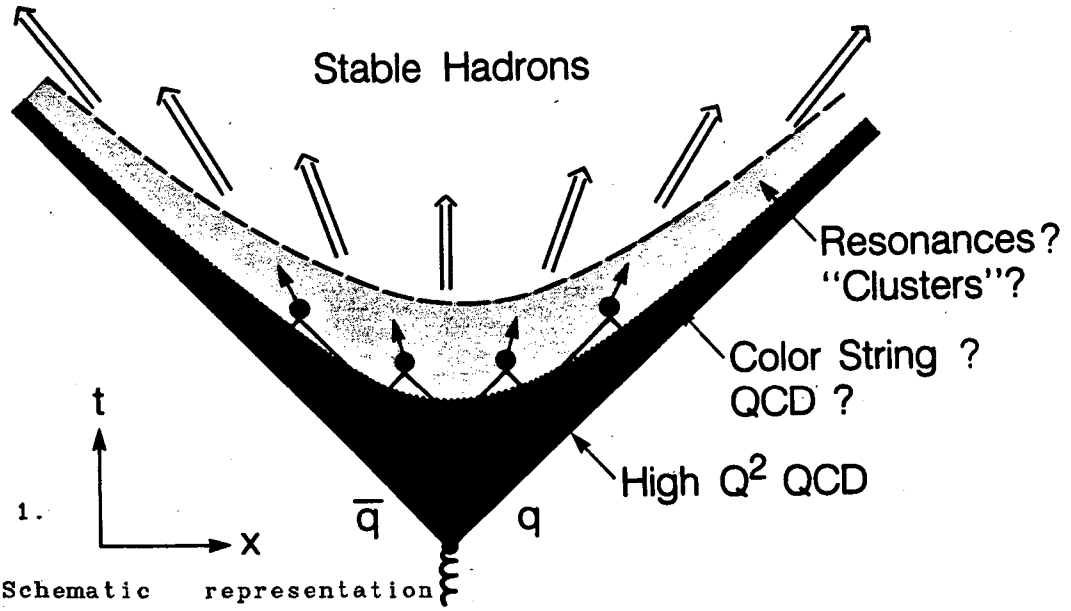

1. Schematic representation of the space-time evolution of the process $e^+e^- \rightarrow$ hadrons

XBL 845-9364

2. Inclusive cross section for charged hadron production (HRS)
a) Fragmentation function $D(z) = (1/\sigma)(d\sigma/dz)$ vs $z = 2p/\sqrt{s}$.
O: All annihilation events
●: 2-jet events only
✱: TASSO data
Full line: LUND model
b) $(1/\sigma\pi)(2E/\sqrt{s})(d\sigma/dx_F) = F(z) \propto zD(x_F)$ vs $(1-x_F)$, where $x_F = 2p_L/\sqrt{s}$. p_L is the momentum component parallel to the thrust axis.

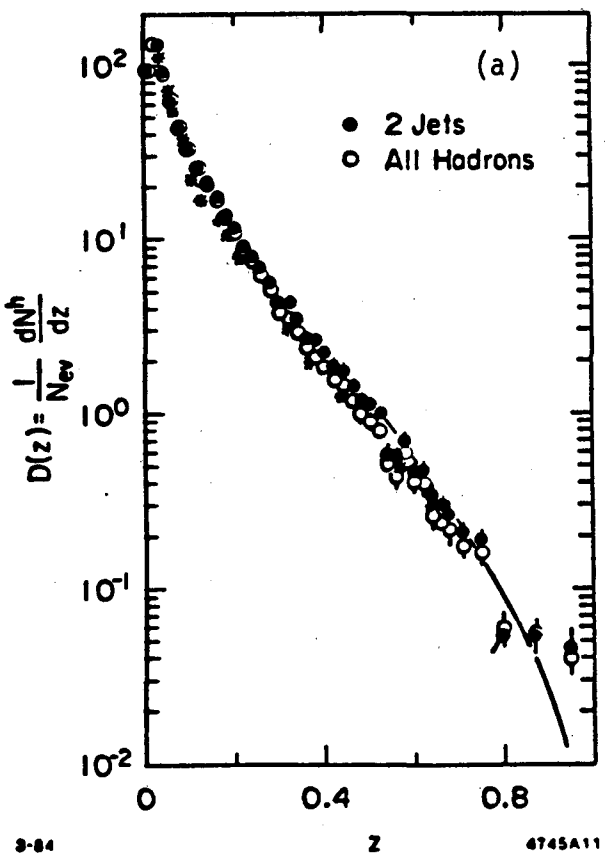

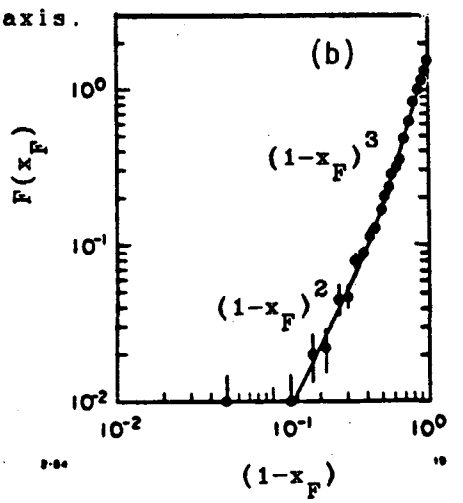

between particles in jets will be discussed as a way to learn more about the confinement region. Finally, the problem of QCD-"tests" will be briefly addressed. Because of the limited space, this paper will concentrate on new, unpublished results.

INCLUSIVE HADRON PRODUCTION. New data from the HRS on inclusive charged hadron production are shown in fig. 2a [8]. These results are based on an integrated luminosity of 20 pb^{-1}, corresponding to about one tenth of the total luminosity collected by the HRS up to now. The fragmentation function $D(z) = (1/\sigma)/(d\sigma/dz)$ is evaluated for all events (O) and for two-jet events (O) which are selected by requiring sphericity and aplanarity values below 0.25 and 0.1, respectively. In the region of overlap, the agreement with earlier data from TASSO [36] is good. The momentum resolution of the HRS of 0.1%*p (in GeV/c) allows for the first time at PEP or PETRA energies the measurement of fragmentation functions in the region $z = 2p/\sqrt{s} \cong 1$. The behavior of D(z) for $z \to 1$ is one of the elementary unsolved questions in the physics of quark fragmentation: perturbative calculations in the quark-parton model predict a non-zero limit for D(z), $zD(z) \propto (1-z)^2 + \mu^2/Q^2$ [9], thereby supporting the old conjecture of Feynman and Field [10], whereas non-perturbative string models seem to require that zD(z) vanishs like a power of (1-z) for $z \to 1$ [1]. Fig. 2b displays zD(z) emphasizing the region $z \to 1$; a power law in (1-z) corresponds to a straight line in this plot. (To be precise: the cross section $F(x_F)$ in fig. 2b refers to $x_F = p_L/p_{max}$, where p_L is the component of momentum parallel to the jet axis; for $x_F \to 1$, x_F and z are equivalent for most practical purposes.) The data exhibit a $(1-z)^2$ dependence for $0.5 < z < 0.9$; in this range the data are consistent both with the "Counting Rules" [9] and the LUND string-model. For the crucial region $z > 0.9$, numerous sources of systematic errors such as minute contaminations of the event sample due to Bhabha or $\tau\bar{\tau}$ events make the analysis very difficult. To this date, no information on the behavior of D(z) for $z > 0.9$ is available. The data shown in fig. 2 prove however, that with the analysis of their full data sample the HRS will be able to make definitive statements; from our point of view, such a measurement and the study of the events with particles at $z > 0.95$ will constitute a major contribution to our knowledge of quark fragmentation.

In the region of moderate $x = 2E/\sqrt{s}$ up to 0.4, the TPC group has recently published final results on inclusive $\pi^{\pm}$, $k^{\pm}$ and $p,\bar{p}$ production [11]; we will discuss here only the scaling behavior of cross-sections at low z, related to searches for gluon-interference effects predicted by perturbative QCD [5,12]. The process of quark fragmentation into a shower of partons is usually considered as a stochastic branching process [13]. However, recent investigations have shown that interference effects are non-negligible, and lead to a strong suppression of soft partons and consequently of soft hadrons in jets [5,12]. This mechanism can be visualized as

follows: a soft gluon, whose wavelength is large compared to the extension of the parton cascade in space-time, will not be able to resolve individual partons. Consequently, the soft-gluon cross-section is not given by an incoherent sum over gluon emission from the many partons in the shower. Instead, the coupling is determined by the net sum of color charges in the shower, resulting in a much smaller cross section. This mechanism provides a very natural cut-off for the evolution of a parton shower. A specific prediction is that the inclusive cross section $(z/\sigma)(d\sigma/dz)$, $z = 2p/\sqrt{s}$, is described by a gaussian in $\ln(z)$; the position of the maximum moves to higher $\ln(z)$ with increasing mass of the object under study. Fig. 3 shows $(z/\sigma)(d\sigma/dz)$ for kaons and protons (pions are not very suitable for these tests, since the pion cross section at low momentum is dominated by pions from resonance decays [14], whereas kaons e.g. will more closely reflect the momentum distribution of strange quarks in the parton shower). The cross section is indeed consistent with a gaussian shape peaking approximately at the z-value predicted by a QCD shower Monte-Carlo simulation [5]. However, an equally good description is given by the LUND model [1] (solid lines), where the behavior of cross sections at small z is essentially governed by longitudinal phase space. We conclude that inclusive spectra alone do not permit a distinction between those two models, especially since Monte Carlo studies show that their results not only do agree at one fixed cms energy, but also exhibit an almost identical energy dependence.

The charged particle cross-sections from the TPC have been supplemented recently by data on π^0 production (fig. 4); charged and neutral pion cross sections agree within errors, yielding $2\pi^0/\pi^{\pm} = 0.92\pm0.14$.

Having measured essentially all stable-particle cross sections, an interesting cross-check is to see if the energy-weighted integrals $\int(Ed\sigma/dx)dx$ add up to the cms energy $\sqrt{s}$. The TPC obtains 12.1±0.7, 3.0±0.3 and 1.5±0.2 GeV for the energies used up to make $\pi^{\pm}$, $k^{\pm}$ and $p,\bar{p}$, respectively. Direct leptons correspond to 0.5±0.1 GeV [37], yielding a total "charged energy" of 59±3%. Photons (including π^0) account for 7.6±.9 GeV (preliminary). All values are corrected for acceptance and effects of initial state radiation. Assuming that neutrons equal protons, and k_L equal k^+ (k_S decays are included in the pions), the energies sum up to 27.7±1.3 GeV, leaving 1.3±1.3 GeV for neutrinos. This number is in fair agreement with the prediction of the LUND model, E_ν = 0.3 GeV. The TPC result on the charged energy fraction agrees with a similar result from the HRS, $E_{charged}$ = 62±4±2%. In their case, momenta are measured and corrections for particle rest masses are obtained from Monte Carlo simulations. Fig. 5 [8] demonstrates that these charged energy fractions agree well with results from e^+e^- annihilation at PETRA and from hadronic interactions at ISR energies.

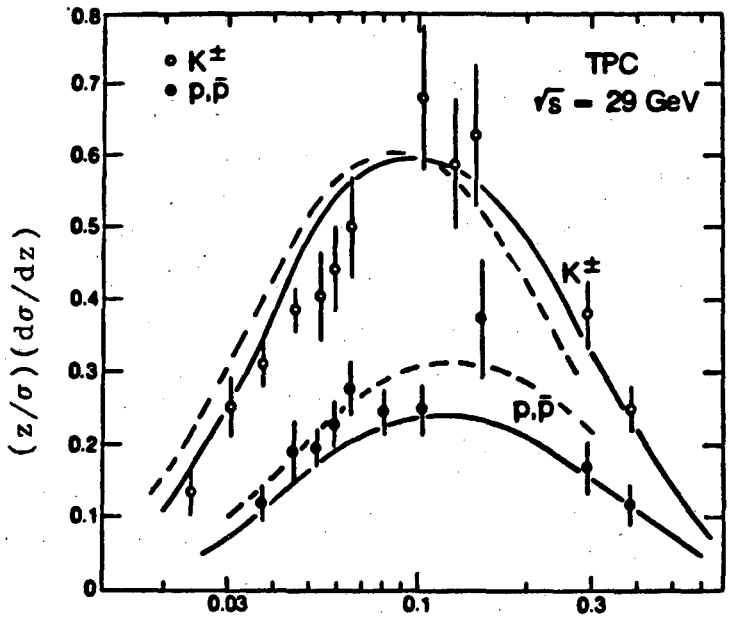

3. Inclusive cross section $(z/\sigma)(d\sigma/dz)$ vs $z = 2p/\sqrt{s}$. Full lines: LUND MC. Dashed lines: Webber MC (TPC).

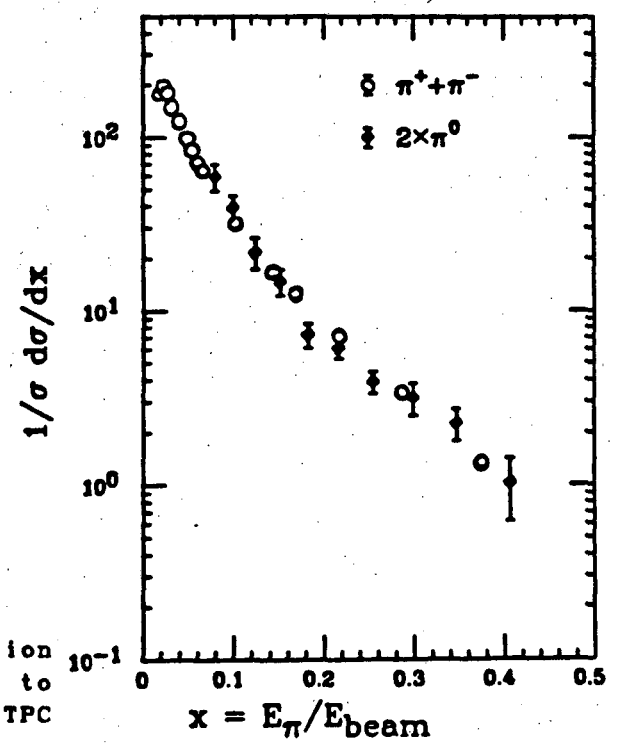

4. Inclusive π^0 cross section vs $x_\pm = 2E/\sqrt{s}$, compared to the $\pi^\pm$ cross section (TPC preliminary).

5. Mean charged energy fraction vs cms energy (HRS)
a) In e^+e^- annihilation
b) Compared to results from pp reactions

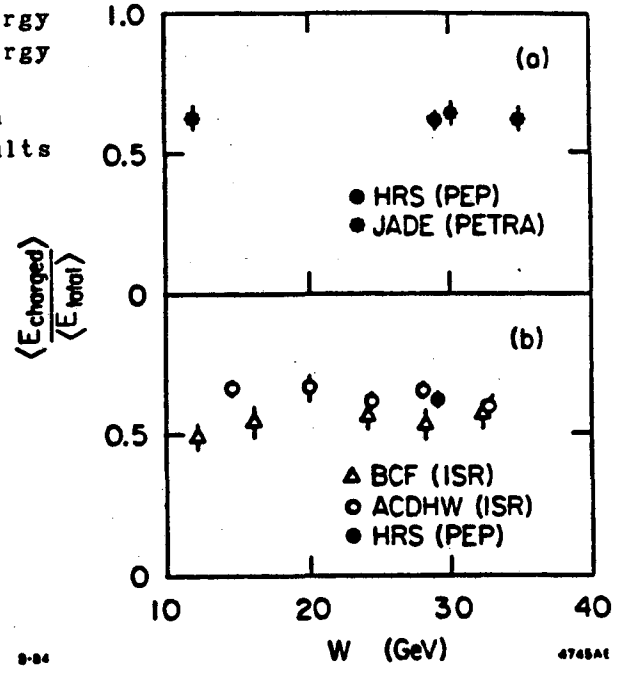

6. Inclusive Ξ production (TPC preliminary)
a) $\Lambda\pi^-$ and b) $\Lambda\pi^+$ mass spectra
b) Inclusive Ξ cross section compared to Λ and proton cross sections
Full lines: LUND model predictions

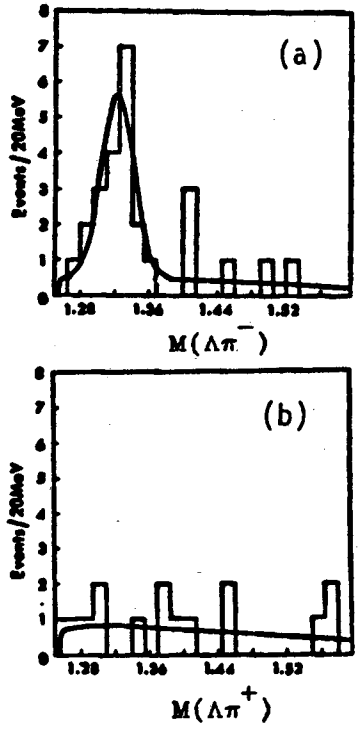

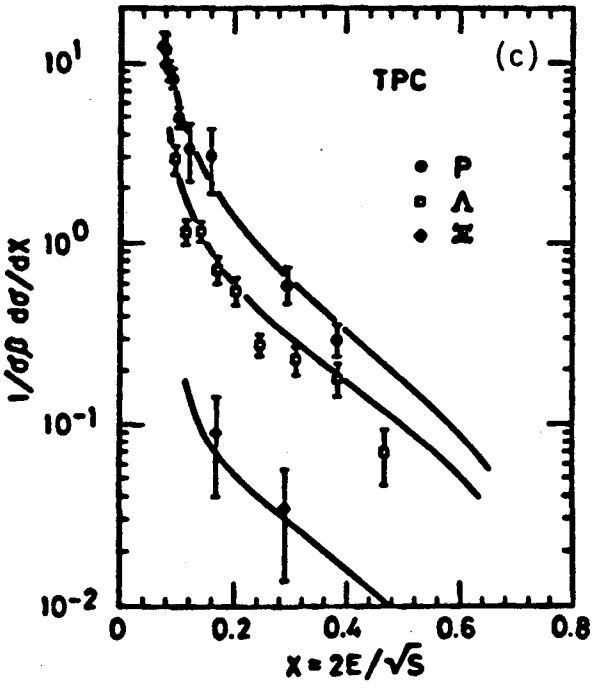

Finally, new data from the TPC are available on Λ and Ξ production. Λ's are detected as usual by reconstruction of a secondary vertex for track pairs whose dE/dx is consistent with a π and p hypothesis. Ξ candidates are selected by requiring another vertex formed by the Λ and a π^-; the $\Lambda\pi^-$ mass distribution (fig. 6a) shows a clean Ξ signal above a small background which can be estimated using $\Lambda\pi^+$ combinations (fig. 6b). The p, Λ and Ξ cross sections are summarized in fig. 6c.

RESONANCE PRODUCTION. Given the fact that all models for hadron production in parton fragmentation contain at least one free parameter determining the mean hadron multiplicity and therefore the general shape of inclusive spectra, one free parameter to adjust strange particle production – in general the mass of the strange quark or a related quantity – and one parameter to tune baryon production, it is obvious that the study of inclusive spectra of stable particles provides little distinctive power between different models. Non-trivial predictions are obtained only for very few quantities like the production rates of Λ, Σ and Ξ as compared to kaon and proton rates.

The study of resonance production opens a wide field of additional tests, such as the dependence of inclusive cross sections on mass and spin of particles. Models like the string picture and the QCD shower approach both make (vague) predictions for mass spectra of the produced objects; the hope is that exploring the realm of resonance production brings us one step closer to the "mysterious" region of color confinement (fig. 1).

For this conference, new results on resonance production have been reported by the DELCO, MARK II and TPC groups. Figs. 7a–d illustrate an analysis of k^{*0} and ρ^0 production by MARK II. Without using any particle identification, $\pi^+\pi^-$ and $k^0\pi^+$ mass spectra are formed. Structures are visible in the k^0 and ρ^0 and in the k^{*0} regions, respectively. The $\pi\pi$ distribution is then fitted by a quartic polynomial and by contributions from k^0, ρ^0, ω and from k^{*0} where the k^- has been mistaken as a π. The resonance shapes are taken from a Monte Carlo simulation. Similarly, the $k\pi$ spectrum is fitted as a sum of k^{*0}, and of reflections of k^{*0}, ρ^0, ω and k^0 due to wrong assignments of particle types. It is assumed that $\sigma(\omega) = (1\pm.5)\sigma(\rho^0)$. A simultaneous fit of the two spectra gives enough constraints to determine the ρ^0 spectrum (fig. 7d, compared to TASSO data [26]), and an integrated k^{*0} cross section. In the range $p > 1$ GeV/c the total cross sections are $0.160\pm0.020\pm0.026$ nb (ρ^0) and $0.139\pm0.022\pm0.037$ nb (k^{*0}). The ratio of k^{*0} (+c.c.) production to ρ^0 production is $0.87\pm0.18\pm0.22$.

In contrast to the MARK II, both the TPC and DELCO detectors make heavy use of their particle identification when searching for k^{*0}. In the DELCO detector, kaons are identified in a threshold Cerenkov-counter, whereas the TPC identifies both decay kaons and

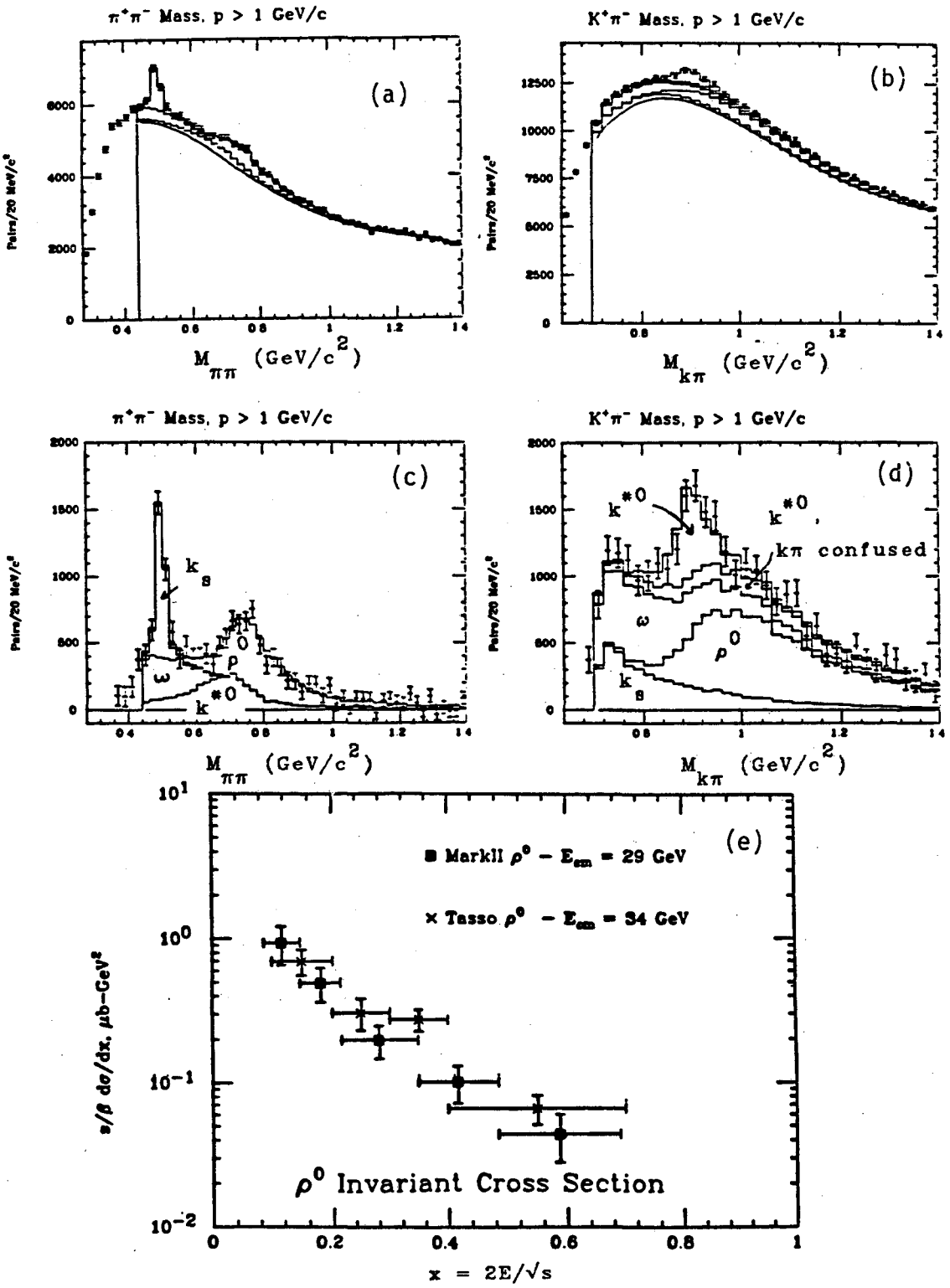

7. Inclusive ρ^0 and k^{*0} production (MARK II preliminary)
a,b) $\pi^+\pi^-$ and $k^+\pi^-$ mass spectra, respectively
c,d) As a,b), but polynomial background subtracted
e) Inclusive ρ^0 cross section vs x, compared to TASSO data

pions by dE/dx measurements. Consequently, those k^* peaks look much cleaner (fig. 8a,b). However the trade-off is a somewhat lower efficiency, which is especially true for DELCO, since only kaons above 2.5 GeV/c can be identified. Both detectors also see clear evidence for ϕ production [15] (fig. 8c,d). The k^{*0} and ϕ cross sections are summarized in fig. 8e. The cross sections from TPC and DELCO are consistent within errors. The agreement with predictions from the LUND model is quite good, although the model overestimates the ϕ cross section at large momentum slightly – an interesting feature since at high x the main source of ϕ's are F decays, according to LUND.

PARTICLE YIELDS. A summary of new results on inclusive particle yields is given in Table 1.

Table 1

Type	Multiplicity	Ref.	Comparison	Ref.
$\pi^{\pm}_0$	10.7±0.6	TPC [11]	10.3±0.4	TASSO
ρ	0.42±0.05±0.07 (p > 1 GeV/c)	MARK II	0.73±0.06	TASSO
$k^{\pm}$	1.35±0.13	TPC [11]	2.0±0.2	
k^{*0}	0.37±0.06±0.10 (p > 1 GeV/c)	MARK II		
	0.39±0.09 (x > 0.1)	TPC		
ϕ	0.084±0.013±0.018	TPC [15]		
p	0.60±0.08	TPC [11]	0.8±.1	TASSO
Λ	0.216±0.013±0.018	TPC	0.28±0.04	TASSO
Ξ	0.025±0.009±0.006	TPC	0.028±0.008±0.008	TASSO
charged	13.1±0.05±0.6	HRS [8]	13.5±0.03	TASSO

All particle yields include c.c. channels. Multiplicities refer to the entire momentum range 0 < x < 1, unless otherwise specified.

Except for $k^{\pm}$ production, the agreement between new results and existing numbers (see summary in [16] for refs.) is good.

PARTICLES AND JETS. The HRS group has carried out an extensive study of properties of jets and of particles in jets [8]. Because of space limitations only the results on longitudinal and transverse distributions of particles in jets will be presented here.

One characteristic property of longitudinal phase space which is shared by string-models for hadronization is the existence of a plateau in the rapidity distribution of particles. The rapidity

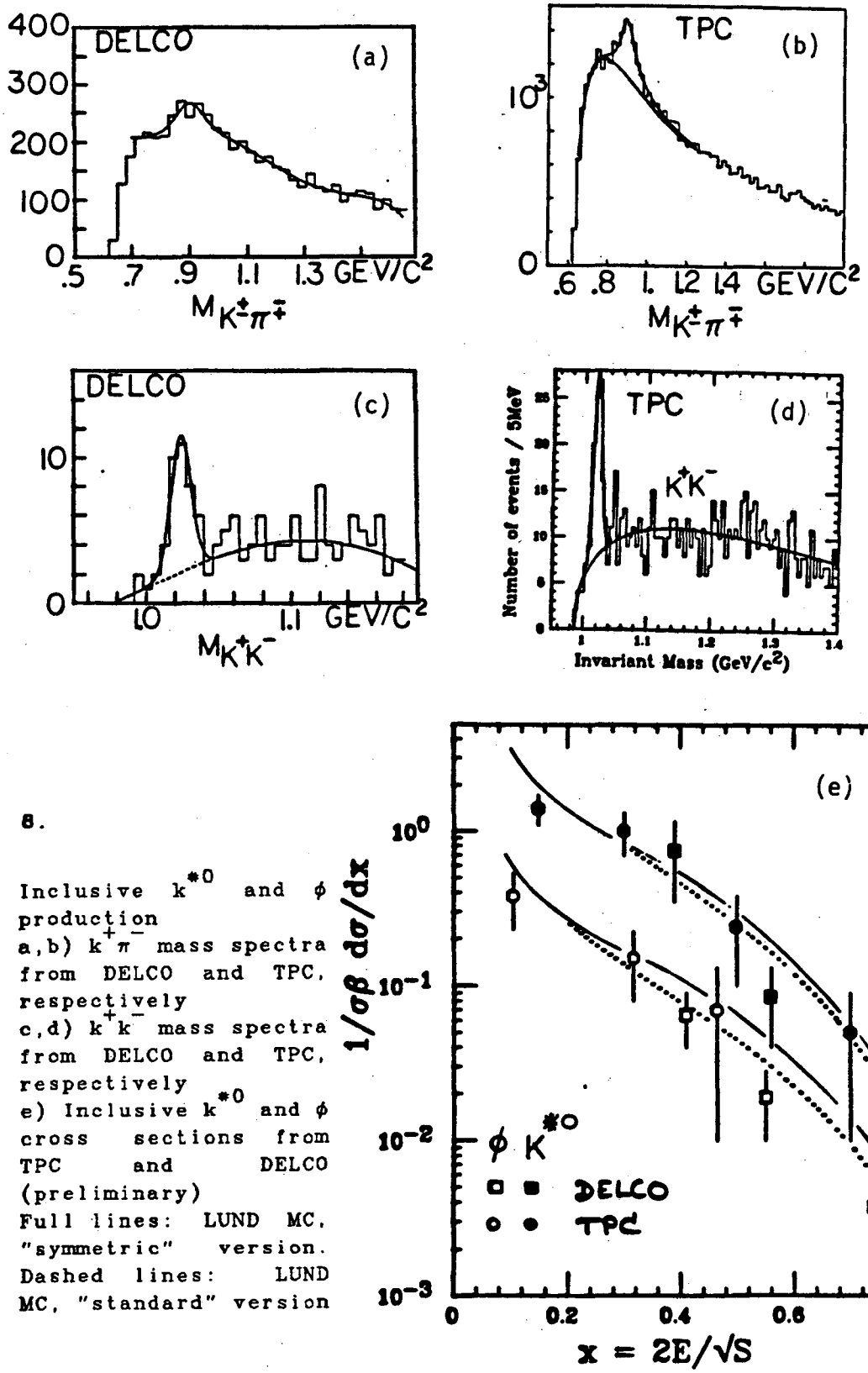

8.

Inclusive k^{*0} and ϕ production
a,b) $k^+\pi^-$ mass spectra from DELCO and TPC, respectively
c,d) k^+k^- mass spectra from DELCO and TPC, respectively
e) Inclusive k^{*0} and ϕ cross sections from TPC and DELCO (preliminary)
Full lines: LUND MC, "symmetric" version.
Dashed lines: LUND MC, "standard" version

distribution of charged hadrons, $(1/\sigma)(d\sigma/dy)$, is shown in fig. 9 for all annihilation events and for 2-jet events only. A rapidity plateau is seen extending over 4 units in rapidity; in the 2-jet sample there is an indication of a dip in $d\sigma/dy$ at $y\cong 0$. Although this is expected in QCD models with gluon interference [5,12], the effect is more likely to be due to an enhancement at $y\cong 2$ due to decay products from charmed hadrons. For comparison, rapidity distributions of hadrons produced in pp interactions at 27 and 52 GeV [17,18] are included.

The distribution of particles in transverse momentum p_T with respect to the thrust axis is shown in fig. 10a, and is compared with the p_T distribution of particles in jets at similar Q^2 from the $p\bar{p}$ collider [19] in fig. 10b. It is surprising that especially the tails of the two distributions agree so well - one would expect higher large-p_T tails for the gluon(?) jets in $p\bar{p}$. Figs. 11a,b display the dependence of $\langle p_T \rangle$ and $\langle p_T^2 \rangle$ on the scaled momentum z; the plots exhibit the well-known "seagull"-effect: mean transverse momenta increase with z at low z; at $z\cong 0.4$ the dependence levels off. Figs. 11c,d,e offer a comparison of this z-dependence with results from other reactions, like low-Q^2 pp interactions [17], deep-inelastic μp scattering [21] and large-p_T jets from the $p\bar{p}$ collider [19]. For the large-Q^2 processes, typical transverse momenta at large z agree rather well, whereas beam jets in pp interactions exhibit smaller p_T's.

The p_T distributions discussed above are averaged over all particle flavors. The TPC group has studied the p_T dependence of cross sections for identified hadrons, notably protons, which are identified by dE/dx measurements [14].

As is well known, the proton fraction among charged hadrons, in the following called f_p, shows a pronounced dependence on the particle momentum p (fig. 12a). The dependence of f_p on transverse momentum p_T with respect to the sphericity axis is shown in fig. 12b-e for different ranges in total momentum p. For momenta below 1.5 GeV, a steep increase of f_p with p_T is observed, in agreement with results from deep-inelastic lepton-nucleon scattering [20]. At high momentum, the p_T-dependence flattens out.

The high value of f_p at large momentum has stimulated speculations that proton production is related to gluon emission [22]; in this case one expects an increase of f_p with p_T. There exists however an alternative explanation for the effects displayed in fig. 12. Assume that the production of primary mesons and baryons is described by simple longitudinal phase space, with a constant baryon fraction. Resonance decays will then soften both the baryon and meson spectra. This softening is more pronounced for mesons, since in a decay of a baryon resonance the decay nucleon will carry a large fraction of the initial momentum, whereas e.g. in a $\rho \to \pi\pi$ decay, the momentum is evenly shared.

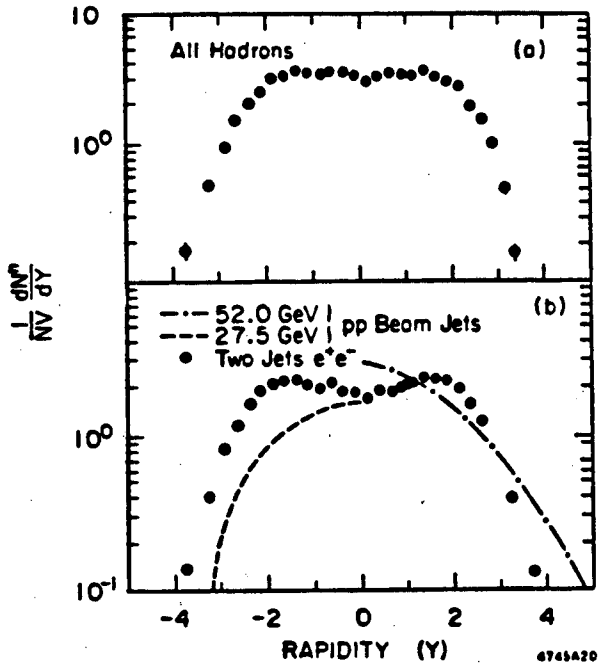

9. Rapidity distributions of charged particles (HRS)
a) All annihilation events
b) 2-jet events only
Dashed and dashed-dotted lines: rapidity distributions of hadrons in pp-interactions at 27 and 52 GeV, respectively. Leading protons are removed in the 27 GeV data.

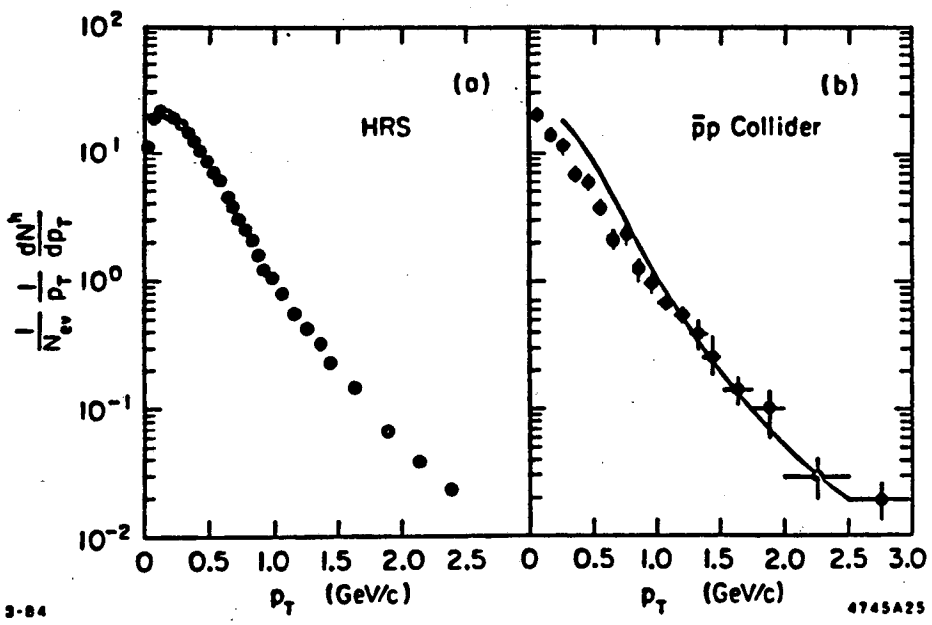

10. a) Distribution of transverse momentum with respect to the thrust axis (HRS)
b) HRS data (full line) compared to p_T distributions measured in jets at the $p\bar{p}$ collider (data points)

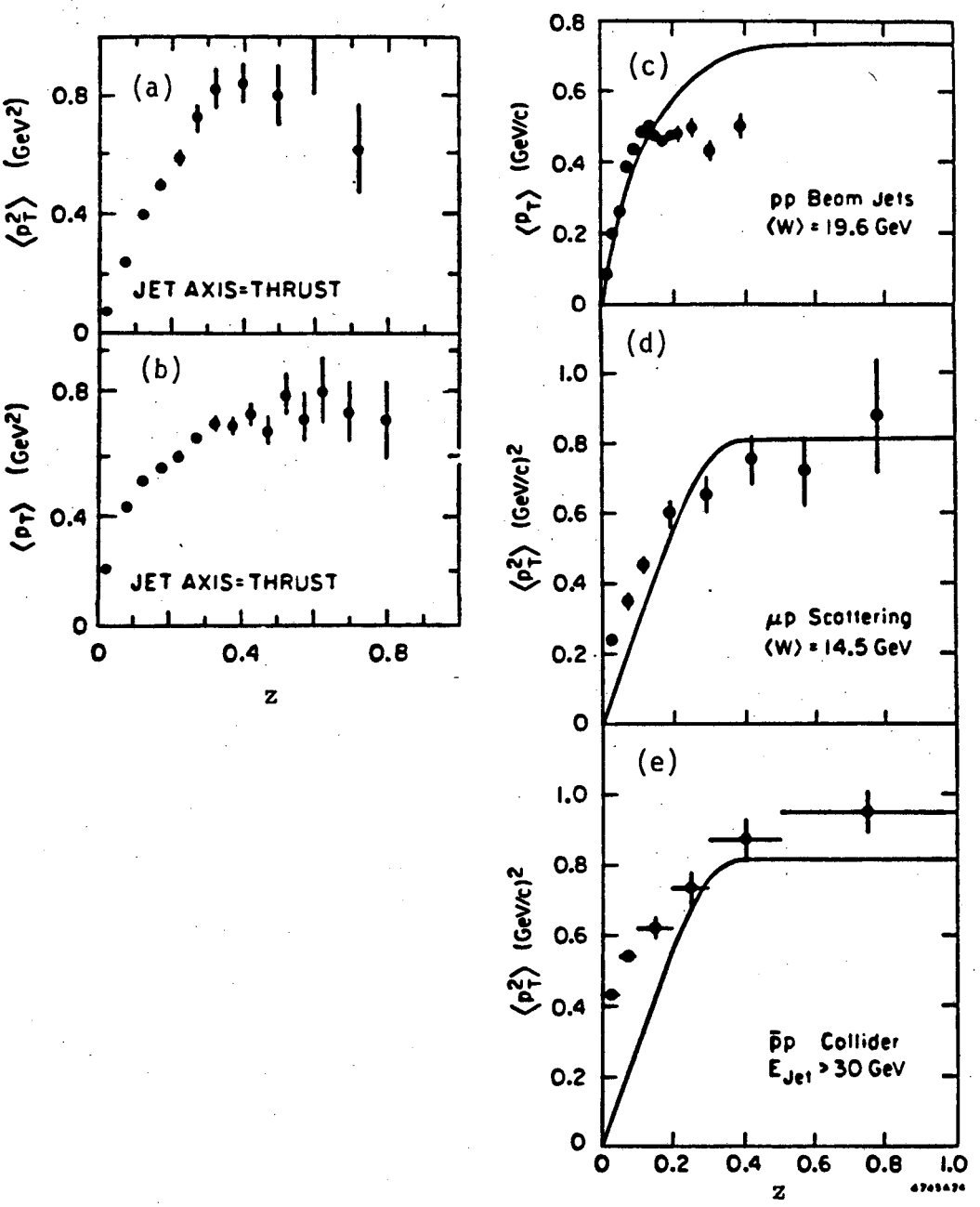

11. Mean transverse momenta vs $z = 2p/\sqrt{s}$ (HRS)
a) $\langle p_T^2 \rangle$ and b) $\langle p_T \rangle$
c) compared to $\langle p_T^2 \rangle$ in low-p_T pp reactions
d) comp. to $\langle p_T \rangle^2$ of particles in jets in μp scattering
e) compared to $\langle p_T \rangle^2$ of particles in jets in $p\bar{p}$ collisions
Solid lines in c-e: e^+e^- (HRS)

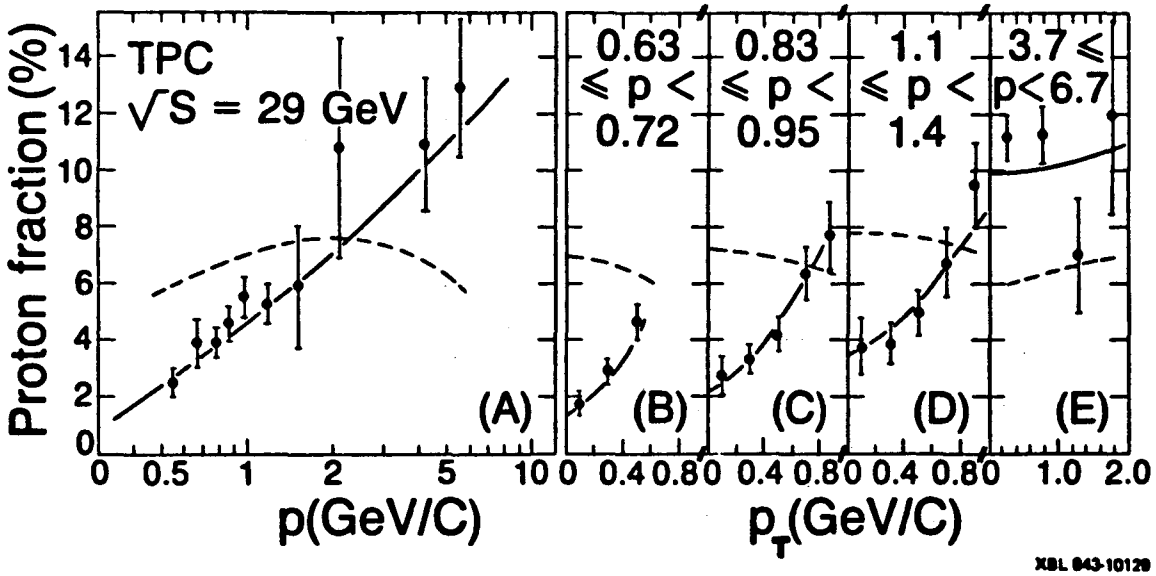

12. Fraction of protons among charged hadrons (TPC)
a) As a function of momentum
b–e) Vs transverse momentum with respect to the sphericity axis, for fixed total momentum
Dashed and full lines: results from LUND MC before and after resonance decays, respectively

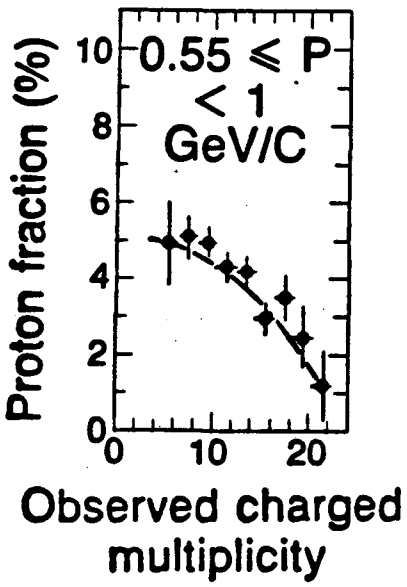

13. Proton fraction at low momentum as a function of hadron multiplicity in the event. Full line: LUND MC (TPC)

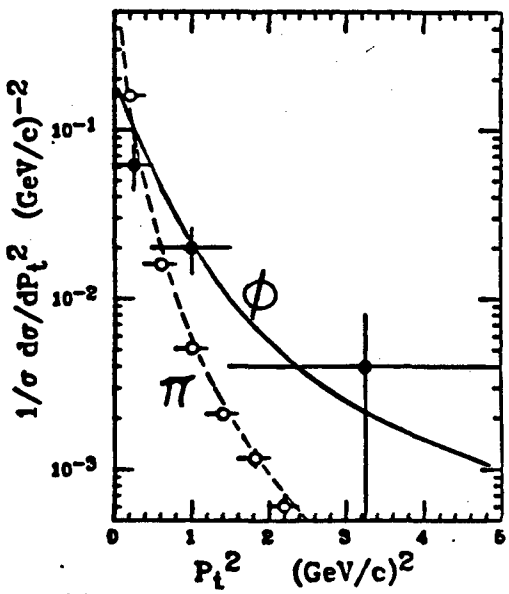

14. Inclusive cross section for ϕ production vs p_T^2. Included is the p_T distribution for $\pi^{\pm}$, scaled by 0.007. Full and dashed lines: LUND MC for ϕ and $\pi^{\pm}$, respectively (TPC).

Explicit calculations using the LUND model confirm indeed that the observed p and p_T dependence of f_p can be obtained from almost flat ratios for the primary hadrons before resonance decays; the dashed and full lines in fig. 12 show the LUND predictions for f_p before and after resonances decay. Hence all the striking variation of f_p with p and p_T can be explained as a consequence of resonance decay kinematics ! There are different ways to check this model: in fig. 13 the fraction of protons among charged hadrons as a function of the hadron multiplicity in the event is shown for low-momentum particles. f_p decreases significantly with increasing multiplicity. This is expected, since high-multiplicity events typically contain a larger fraction of vector mesons, resulting in a strong increase in the number of low momentum decay pions and hence in a corresponding decrease in f_p. The effect is quantitatively reproduced in the LUND model (full line).

The same line of reasoning applies to any comparison of p and p_T distributions of light and heavy particles; the heavy particles will be closer to what is primarily produced in the confinement process and will have less steep p and p_T distributions. This is illustrated in fig. 14, where p_T distributions for pions and ϕ's are compared [15]. Again, the LUND model gives a very good description of the distributions.

Obviously, many properties of hadron production can be explained in such a simple model, assuming essentially that all primary hadrons have similar momentum spectra (except for "leading" particle effects, of course), and a universal p_T distribution. It is thus obvious that heavy particles are better, more direct probes of fragmentation phenomena than light mesons; they suffer less from the dilution of information due to resonance decays.

HEAVY QUARK FRAGMENTATION. The physics of heavy quark fragmentation combines several interesting aspects: in trying to explore the effects of confinement forces, ideally one would like to have a "test" parton whose momentum is known before and after it interacted with the forces of a confining color field. A heavy quark comes close to that ideal: its initial momentum is essentially given by the beam momentum, and it can be unambiguously identified in the final state. Apart from its role in fragmentation phenomenology, the study of heavy quark production serves to explore properties of heavy quarks and their decays, and to study electroweak effects.

Heavy quark fragmentation is clearly the domain of the HRS detector, which is where the bulk of new data originates. It's excellent momentum resolution enables the HRS to detect $D^0 \to k^- \pi^+$ directly as a peak in the $k\pi$ mass spectrum (fig. 15a). The peak is localized at a mass of 1861±2 MeV and has a width of 13 MeV. No particle identification is used; cuts on $z = 2E_D/\sqrt{s}$ and on the decay angle θ_π, $|\cos(\theta_\pi)| < 0.7$ reduce combinatorial backgrounds.

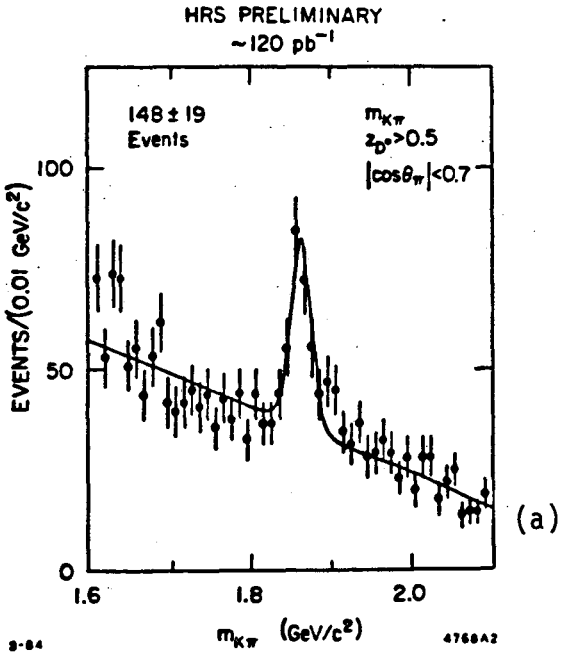

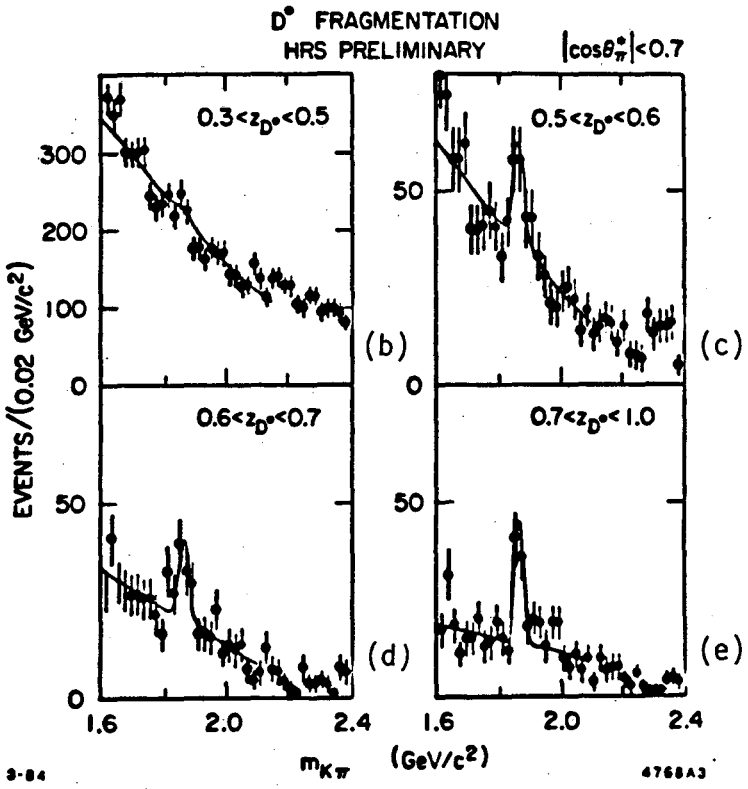

15. $k\pi$ mass spectra (HRS preliminary)
a) $z_{k\pi} > 0.5$ (with $z = 2E/\sqrt{s}$)
b–e) $k\pi$ mass spectra for different z intervals

In fig. 15b-e the $k\pi$ mass distribution is shown for different intervals in z; for the lowest z-bin, $z < 0.5$, only an upper limit for the cross section can be given.

The "classical" method [23] to study D production concentrates on the decay $D^{*+} \to D^0 \pi^+$, $D^0 \to k^- n\pi^\pm$. Since the mass resolution in the D^*-D mass difference is dominated by the precision with which the π momentum is measured, the resolution in the D^*-D mass is greatly improved as compared to the D mass resolution. Fig. 16 shows HRS results on the D^{*+}-D^0 mass difference for the decay channels $D^0 \to k^-\pi^+$, $k^-\pi^-\pi^+$, $k^-\pi^+\pi^0$. In the first two decay modes, the mass of the $k^- n\pi^\pm$ system is required to coincide with the D mass. In the last mode, the π^0 is not detected, and the $k^-\pi^+$ satellite enhancement is used to select $k^-\pi^+$ combinations. In the charged decay modes, a resolution of less than 1 MeV on the mass difference is obtained! The HRS also observes D^+ directly via $D^+ \to k^-\pi^+\pi^+$ (fig. 17).

The acceptance corrected D cross sections from the HRS are shown in fig. 18; here z is defined as $2E/\sqrt{s}$. The D^{*+} and D^0 agree within errors, and the D^{*+} data are consistent with data from MARK II [23] and TASSO [24]. The D cross section peaks at $z \cong 0.5$-0.6, confirming that heavy mesons tend to carry a large fraction of the heavy quarks momentum, as expected in the quark-parton model on the basis of kinematical arguments [25]. The integrals over the inclusive cross sections normalized to the $\mu^+\mu^-$ cross section give (preliminary) R-values of $R(D^0) = 1.65\pm0.6$ $R(D^+) = 0.8\pm0.4$ and $R(D^*) = 2.0\pm0.2$. These values include the charge conjugated channels; $R(D^*)$ includes both D^{*+} and D^{*0}, assuming isospin symmetry. The errors include uncertainties in the D branching ratios. This source of systematic error and most acceptance effects cancel, if the ratio $R(D^0)/R(D^*)$ is considered. For the region $z > 0.4$, the HRS obtains $R(D^0)/R(D^*) = 0.6\pm0.2$.

The ratio of D^* to direct D production provides an interesting test of the spin dependence of hadron cross sections. Naively, one expects a ratio of 3/1 for the relative rates of vector/pseudoscalars. In the case of ρ/π and k^*/k, the observed ratios are closer to 1 [16]. The string model [1] provides an explanation for the deviation from spin counting: $q\bar{q}$ production in a string can be described as a tunneling process, and the wavefunctions of mesons favor tunneling into scalar states as compared to vector states. The suppression of vector particles is predicted to be of the order of the vector/scalar mass ratio, and should be virtually absent for the D system. The measured D^0/D^* ratio strongly constrains the probability of D^* vs D production. Taking into account that observed D^0's are fed by direct D^0 production, by 100% of the D^{*0} decays and by about 44% of the D^{*+} decays [27], observed D^0/D^* ratios of 1.2, 0.9 and 0.7 are expected for ratios of direct D/D^* production of 1/1, 1/3 and 0/1, respectively. From the HRS data, one concludes that D^* production

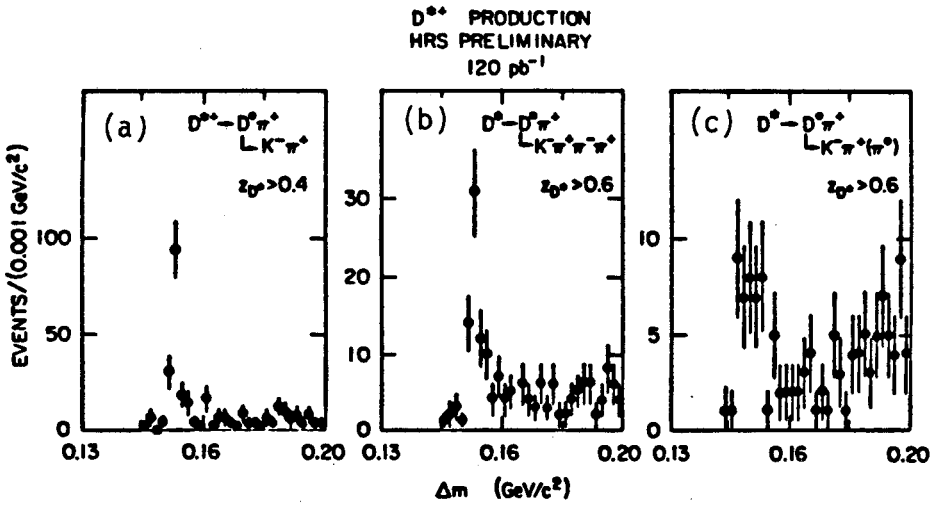

16. D^* - D mass difference plot (HRS preliminary)
a) Selecting $D^0 \to k^-\pi^+$ candidates
b) Selecting $D^0 \to k^-\pi^+\pi^-\pi^+$
c) Selecting $D^0 \to k^-\pi^+\pi^0$ (π^0 not seen), using the satellite enhancement at $m_{k\pi} \simeq 1.5$ GeV

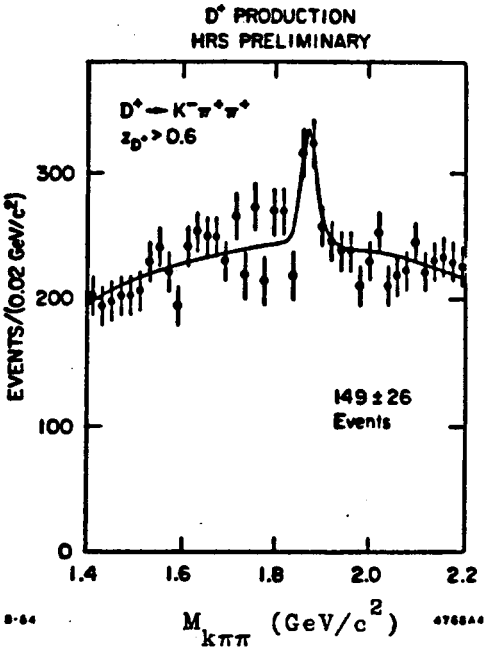

17. $k^-\pi^+\pi^+$ mass spectrum for $z > 0.6$ (HRS preliminary)

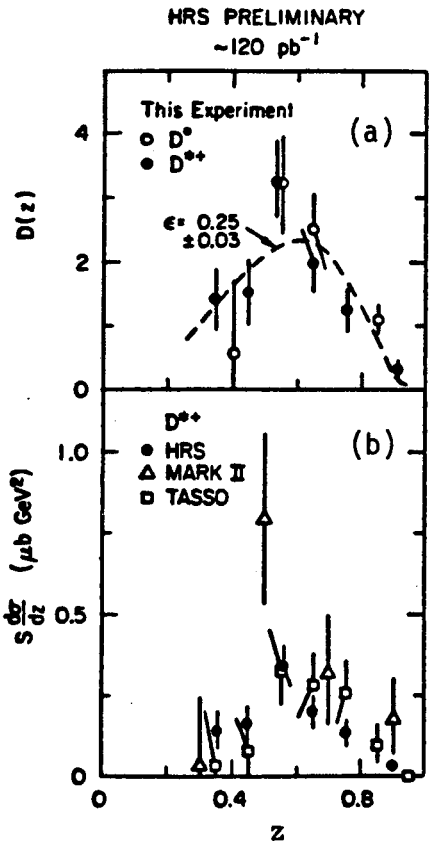

18. Inclusive D and D^* production cross sections (HRS preliminary)
a) D^0 and D^{*+}.
b) D^{*+} data compared to MARK II and TASSO data

is strongly favored as compared to direct D production. Taking into account the uncertainties in the $D^{*+} \to D^0$ branching ratio, a (1 s.d.) upper limit for to ratio of direct D to D^* production of about 1/4 can be derived (in contradistinction to earlier results based on lower statistics, which were consistent with significant direct D production [16])

For the first time, results on D^* production became available from the TPC. Fig. 19a shows the $D^{*+}-D^0$ mass difference distribution for the decay channels $D^0 \to k^- \pi^+$, $k^- \pi^+ \pi^- \pi^+$ and $k^- \pi^+ \pi^0$. Despite the limited momentum resolution of the TPC - ≈3.5%*p - a good signal-to-background ratio is maintained since the decay particles are identified by dE/dx measurement, thereby reducing the combinatorial background by more than one order of magnitude. Preliminary results on the shape of the D^* momentum spectrum are consistent with other detectors - the fragmentation function of charmed quarks into D^* peaks at z≅0.6, with $\langle z \rangle = 0.58 \pm 0.02$ (fig. 19b).

Using the same technique, and relying heavily on its good particle identification, the TPC has searched for other charmed hadrons. Most interesting is the search for the F^* decaying into $F\gamma$, $F \to k^+ k^- \pi^+$. The F^* is expected to show up as a peak in the distribution of the mass difference $\Delta M = M_{kk\pi\gamma} - M_{kk\pi}$ displayed in fig. 19c (preliminary). The full curve represents ΔM, with $M_{kk\pi}$ in the F range, $M_{kk\pi} = 1.96 \pm 0.12$ GeV. An excess of 35±12 events is observed at $\Delta M \cong 150$ MeV, which disappears if the $M_{kk\pi}$ window is moved away from the F region (dashed line). The width of the peak is consistent with the detector resolution. Forming the $M_{kk\pi}$ distribution and selecting combinations in the ΔM peak, a 3 s.d. signal at the F mass is observed. No clear evidence for a $\phi\pi$ decay mode is seen, but upper limits on this mode are consistent with results from CLEO [28]. Further investigation and consistency checks of this F^* candidate are in progress.

FLAVOR CORRELATIONS. A powerful way to study the action of the forces leading to quark confinement is offered by the study of quantum number correlations. A particular quantum number is used to "label" a pair of quarks produced from the vacuum, and to find the final state particles containing these quarks. This technique has been used previously to investigate charge-correlations in hadronic interactions [29] and in e^+e^- annihilation [30]. New data on such "flavor-tagged" correlations are available from the TPC.

The method is illustrated in fig. 20a using charge-weighted $\pi\pi$ correlations as an example. For each event, the sphericity axis is calculated and particle rapidities are calculated with respect to this axis, using particle masses derived from dE/dx measurements. Events are chosen which have a π^- at large positive rapidities ($1.5 < y < 4$). Shown in fig. 20a is the net charge density of additional pions in the event, i.e. $(1/\sigma)(d\sigma_{\pi^+}/dy - d\sigma_{\pi^-}/dy)$ (the

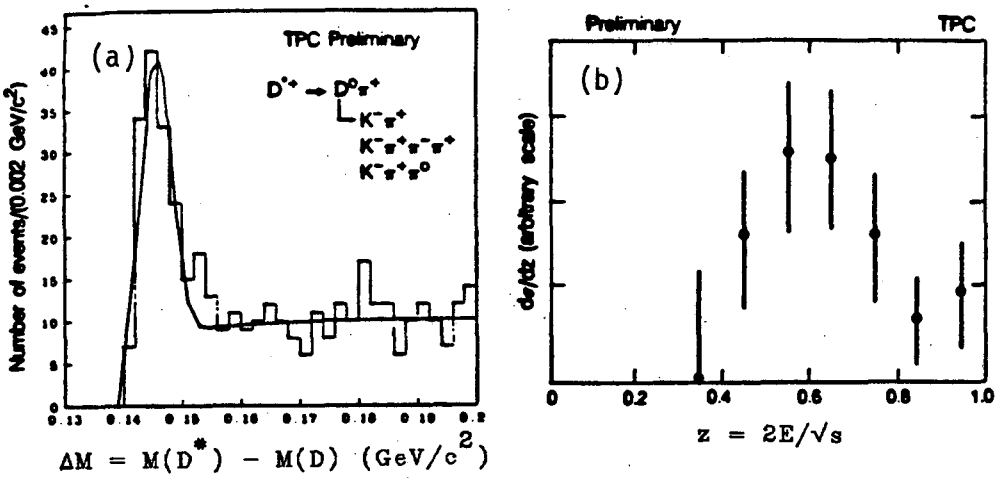

19. Preliminary TPC results on heavy quark fragmentation
a) $D^{*+} - D^0$ mass difference distribution, selecting $D^0 \to k^-\pi^+$, $D^0 \to k^-\pi^+\pi^-\pi^+$ and $D^0 \to k^-\pi^+\pi^0$
b) Inclusive D^{*+} production vs z = 2E/√s
c) $k^+k^-\pi^\pm\gamma - k^+k^-\pi^\pm$ mass difference. Full line: for $kk\pi$ systems in the F region, $M_{kk\pi}$ = 1.96±0.12 GeV. Dashed line: for $kk\pi$ systems above and below F region

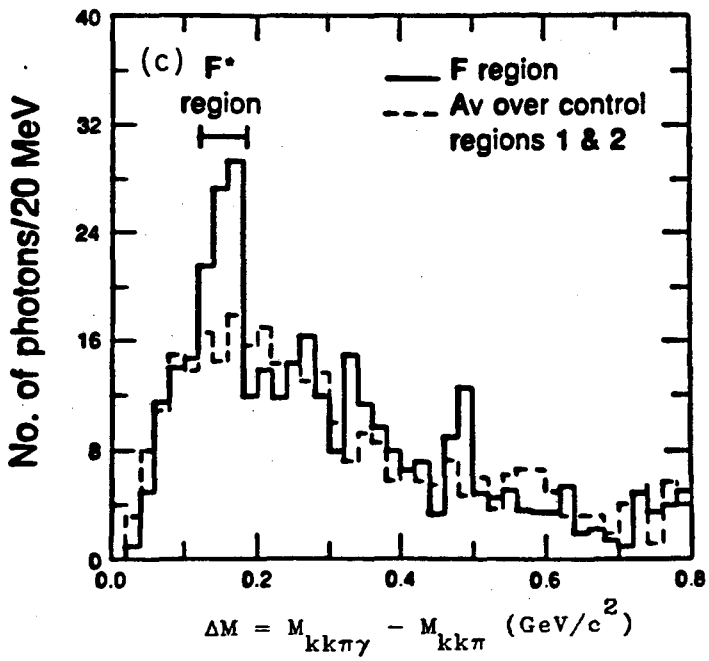

σ in the denominator is the total cross section to produce events with a "test" particle). This quantity is most easily understood as the answer to the following question: "Since we pick out a π^- at large y, there must be an excess of one unit of positive charge among the other particles in the event. How much of this excess is carried by other pions, and where in rapidity is it localized ?". Or, given our faith in the quark model, we might ask: "The test π^- contains two negative partons, a quark and an antiquark. Since quarks are produced pairwise, there has to be an excess of positive partons somewhere, and from the difference in rapidity between the π^- and the particle containing the positive parton we can estimate the size of the momentum transfers involved in the process !" As evident from fig. 20a, there are two different types of correlations: most of the charge of the π^- is compensated locally in rapidity. In addition there is a small, but significant long-range charge correlation. The strong short range correlation shows that most of the quarks making up pions are produced in soft, low-Q^2 processes. Such a process is e.g. quark-antiquark production in a color force field, another example is particle production in resonance decays. Indeed studies using the LUND model suggest that most of the short-range correlation in fig. 20a is due to decays like $\rho^0 \to \pi^- \pi^+$, i.e. we are testing mainly the region of resonance decays and not the region of confinement dynamics (fig. 1)! The long-range correlation is indicative of a large-Q^2 process, the obvious candidate being the initial creation of a quark-antiquark pair by the virtual photon. In this case one of the initial quarks is contained in the "test"-π^-, the other one appears at large rapidity in the opposite jet. Both color-string models (LUND [1]) and QCD branching models (Webber [5]) give an approximate description of these phenomena (fig. 20a).

A more interesting case are kaon correlations, since there the contributions from resonance decays to the short-range correlation are smaller (mainly from $\phi \to k^+k^-$ and $F \to k^+k^- + x$). Fig. 20b displays the charge density of additional kaons in events with a "test" k^- at large positive rapidity, i.e. $(1/\sigma)(d\sigma_{k^+}/dy - d\sigma_{k^-}/dy)$. This quantity shows where in rapidity the strangeness of the "test" k^- is compensated. All flavor correlations shown in fig. 20 are corrected for acceptance and particle misidentification (the typical purity of the kaon sample is $\approx$80%); the systematic errors associated with these corrections are included in the error bars.

As compared to the pion correlations, the pattern has now changed: long and short range correlations appear at approximately equal strength. The long range correlation is caused by events with initial charm and strange quarks, whereas the short range k^-k^+ correlation indicates the production of $s\bar{s}$ pairs from the vacuum by a soft process. Hence fig. 20b illustrates the two different scales of momentum transfers involved in the process $e^+e^- \to$ hadrons: the initial production of a quark pair from the large-Q^2 virtual photon leads to a large separation of quantum numbers in rapidity

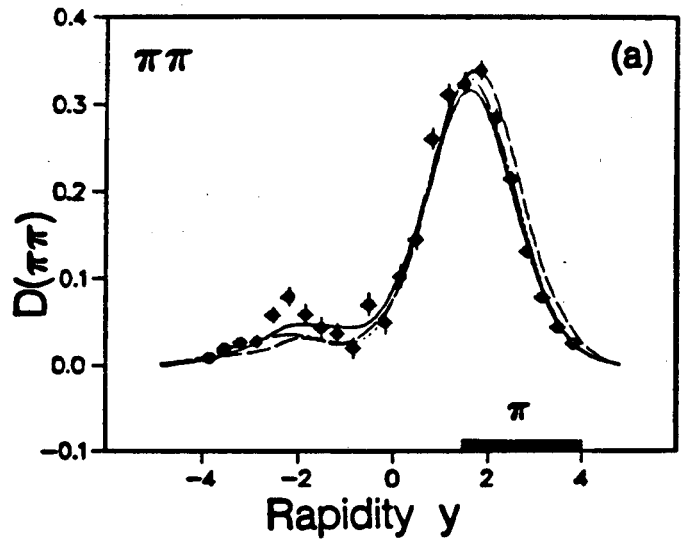

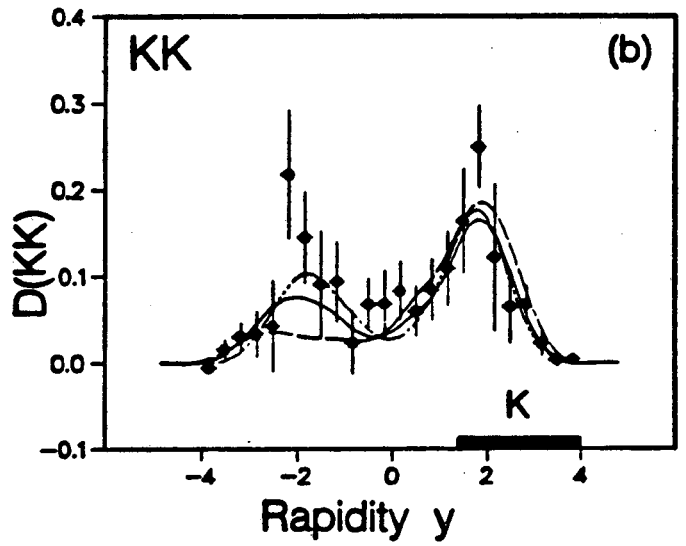

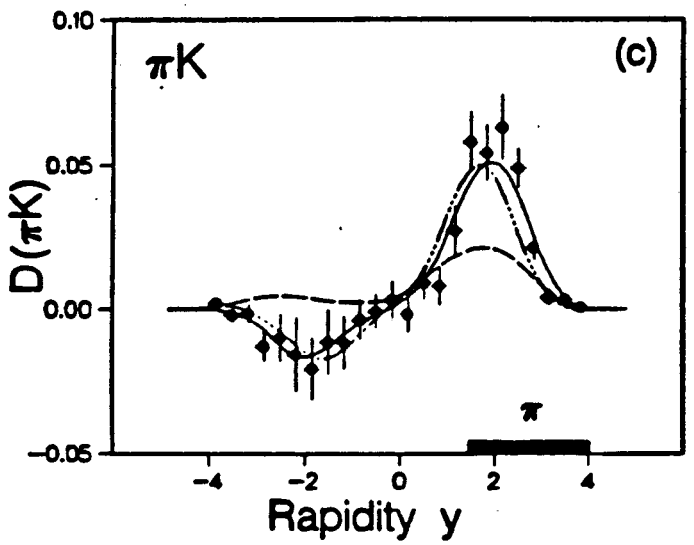

Flavor-tagged rapidity correlations (TPC preliminary)
a) Charge density $D(\pi\pi)$ of additional pions in events with a "test"pion at high rapidity ($1.5 < y_\pi < 4$)
b) Charge density $D(kk)$ of additional kaons in events with a "test"-kaon at high rapidity
c) Charge density $D(\pi k)$of additional kaons in events with a "test"-pion at high rapidity
Full and dashed-dotted lines in a-c: predictions by the LUND and Webber MC's, respectively. Dashed lines: LUND MC with a soft fragmentation function for heavy quarks

and to long-range correlations, whereas the basic confinement process operates at low Q^2 and creates short-range correlations in rapidity. Both the LUND-model and QCD jet models incorporate these assumptions and give very good descriptions of the data. (It may not be obvious that flavor creation in a QCD shower happens at low Q^2; the reason is that due to the large gluon-gluon coupling the shower proceeds mainly by gluon production. Most quarks are produced at the very end from low Q^2 gluons, which are forced to split into quark-antiquark pairs.)

Obviously the method of charge-weighted rapidity correlations can also be used to study πk correlations. Fig. 20c shows the net charge density among kaons in events with a high-rapidity π^-. The resulting pattern of correlations is quite surprising: apart from the familiar positive short-range correlation, a negative long-range correlation is observed, i.e. events with a π^- at high rapidity in one jet have an excess of k^- at high rapidities in the opposite jet! This effect can be interpreted in term of $c\bar{c}$ production at the primary vertex: the $\bar{c}$-quark fragments into an anti-charm meson, like a D^-, which decays e.g. into $k^+\pi^-\pi^-$; therefore an excess of k^+ is seen close to the π^-. The c-quark in the opposite jet forms a charmed meson decaying into a k^-+x, giving rise to the long-range $\pi^- k^-$ correlation. Again the Monte-Carlo models provide a quantitative description.

"QCD TESTS": STRINGS OR NO STRINGS?. Testing the predictions of perturbative QCD concerning gluon bremsstrahlung from accelerated quarks has developed as one of the major goals in the physics of e^+e^- annihilations. The experimental(?) problem is obvious from fig. 1: the region of interest - high Q^2 QCD - is hidden behind the regions of low-Q^2 color confinement and of resonance decays. Although the main predictions of QCD, like the angular distribution of gluon radiation, have been verified, investigations by the CELLO group [31] and others [32] have shown that determinations of the strong coupling constant α_s depend strongly on the assumptions concerning the fragmentation process. Two models yielding extreme values of α_s are the LUND string-model and the so-called independent-fragmentation schemes like the Hoyer- or Ali-models [33,34]. For events with a radiative gluon, the LUND model assumes that a kinked color force field is spanned from the quark to the gluon and then to the antiquark. The fragmentation is described in the local rest frame of the color string. Fragmentation products are then boosted back to the e^+e^- cms. In contrast, independent-fragmentation models assume that each parton fragments independently of all others, and that the process is described in the overall cms. Two effects induce the need for different values of α_s when the two types of models are to reproduce experimental data: In the LUND model, the lorentz-boost between the color-anticolor rest frame and the cms tends to smear the jet structure, making 3-jet events look more 2-jet like. On the other hand, independent-fragmentation schemes inherently don't

conserve energy and momentum, since each zero-mass parton fragments independently into a jet whose average mass is non-zero. Some of the schemes used to patch up momentum conservation try to adjust the momentum of a gluon jet to the momentum of the initial gluon, thereby systematically increasing the effective gluon energy.

The obvious solution to this problem is to try to distinguish experimentally between those two schemes. Or to put it clearly: can an obviously inconsistent (because it is not lorentz invariant) scheme like the independent-fragmentation model be ruled out in favor of string-like models, which at least exhibit internal consistency ?

In a recent analysis by the TPC group, experimental data are compared to predictions from LUND Monte Carlo program, which was used either in its string-mode or in a mode emulating independent-fragmentation schemes. As a first step, the model parameters governing the longitudinal spectra ("A","B"), mean transverse momenta ("σ_q"), and the 3-jet rate ("α_s") were determined for each of the two modes from multi-parameter fits of model predictions to the data. Experimental distributions were classified in three groups: data mainly sensitive to A and B, to σ_q and to α_s, respectively. The optimization was performed for different combinations of one data set from each group; the constants A,B e.g. can be constrained either by fitting to inclusive spectra or to multiplicity distributions. The results of the fits for the two parameters α_s and σ_q are summarized in fig. 21. Within each mode, the fit results corresponding to different experimental data sets essentially agree within errors; the values for α_s obtained with the string- and with the independent-jet version of the model differ significantly. These values agree with results from CELLO and TASSO obtained by similar methods. Both variants of the model give almost equally good fits to the data.

In search for experimental evidence in favor of one or the other models, the TPC follows an analysis by the JADE group [35]. Using a cluster algorithm, 3-jet events are selected. Particle momenta are then projected onto the event plane, and the angular distribution of particles is plotted. The jet with the highest momentum is defined as $\phi = 0$; the jet with the second highest momentum has $\phi < 180$ degr., and the jet with the lowest momentum - typically the gluon jet - is between $\phi = 180$ and $\phi = 270$ degr.. A string model, where particles are boosted into the regions between quark (or antiquark) and gluon jet, is characterized by a depletion of the particle density in the region between the quark and the antiquark jet, at $\phi \cong 90$ degr.. Only relevant for non-relativistic particles, the effect should be most pronounced for heavy hadrons like kaons or protons. The angular distribution of such particles is shown in fig. 22 in comparison with Monte-Carlo predictions. In agreement with the string model, the valley between quark and antiquark jet is deeper than the valley between quark and gluon

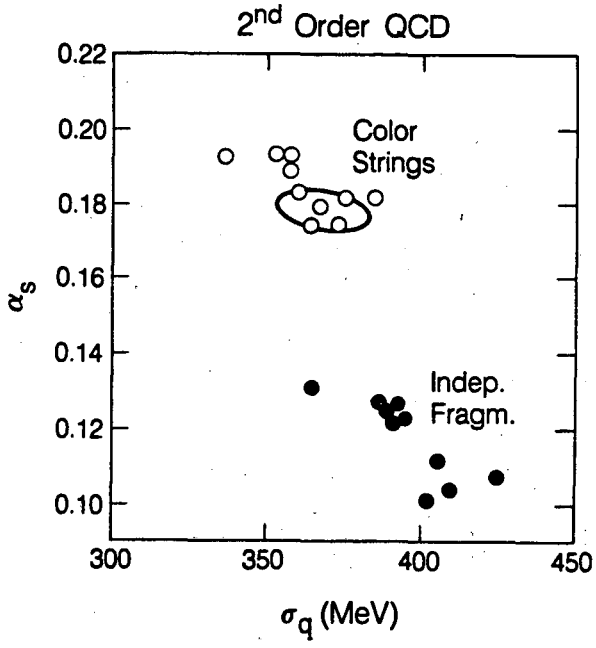

XBL 845-9366

21. Distribution of optimum values for the model parameters α_s and σ_q for the string-fragmentation and the independent fragmentation mode of the LUND generator. The different data points correspond to different sets of experimental distributions used to constrain the parameters. The oval represents the typical statistical error (TPC).

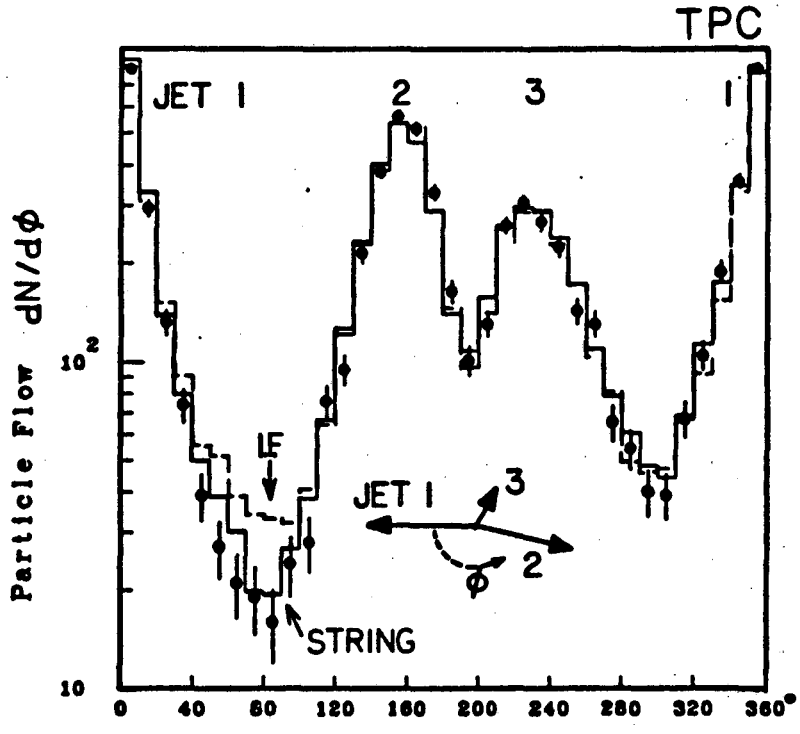

22. Particle flow as a function of the angle ϕ in the event plane for particles in 3-jet events. $\phi = 0$ corresponds to the highest momentum jet. Only heavy particles ($k^{\pm}, k^0, p, \bar{p}$) are used. Full and dashed lines: predictions of the LUND generator used in its string- and independent-fragmentation modes, respectively (TPC)

(-enriched) jet, confirming earlier conclusions by the JADE group [35].

SUMMARY. The results reported from the detectors at PEP in this paper, and by other contributions to this conference, document that PEP provides an active and competetive environment for e^+e^- physics. The special capabilities of PEP-detectors such as the HRS with it excellent momentum resolution, the TPC with its particle identification and the PEP-9 2-photon detector open new possibilities and areas of research even in a field as crowded as the physics of e^+e^- reactions at PEP and PETRA energies.

Considerable progress has been made at PEP in the measurement of inclusive stable-particle and resonance production. Longitudinal and transverse distributions of particles in jets have been presented, both for inclusive charged hadron production, baryon production and resonance production. Charmed meson production has been investigated extensively by the HRS. The flavor-tagged particle correlations reported by the TPC group were discussed as a new tool to investigate fragmentation dynamics. It is observed that the study of heavy particle production in jets provides increased sensitivity to the basic fragmentation phenomena, as evidenced e.g. in a comparison of fragmentation schemes by the TPC.

This work was supported by the Department of Energy under contract no. DE-AC03-76SF00098.

REFERENCES

1. B. Andersson et al., Phys. Rep. 97C, 31 (1983)

2. R.D. Field, S. Wolfram, Nucl. Phys. B213, 65 (1983)

3. P. Mazzanti, R. Odorico, Z. Phys. C7, 61 (1980)

4. T.D. Gottschalk, Nucl. Phys. B214, 201 (1983)

5. B. Webber, CERN-TH-3713 (1983)

6. G. ALtarelli, G. Parisi, Nucl. Phys. B126, 298 (1977)

7. J.D. Bjorken, "Current Induced Reactions" (Springer, Berlin, Heidelberg, New York, 1976)

8. HRS Collab., D. Bender et al., to be submitted to Phys. Rev. D

9. G.R. Farrar, D.R. Jackson, Phys. Rev. Lett. 35, 1416 (1975)

10. R.D. Field, R.P. Feynman, Nucl. Phys. B136, 1 (1978)

11. TPC Collab., H. Aihara et al., Phys. Rev. Lett. 52, 577 (1984)

12. A.H. Mueller, Nucl. Phys. B213, 85 (1983); B228, 351 (1983)
Yu.L. Dokshitzer, V.S. Fadin, V.A. Khoze,
Phys. Lett. 115B, 242 (1982)

13. K. Konishi, A. Ukawa, G. Veneziano, Phys. Lett. 78B, 243 (1978)

14. TPC Collab., H. Aihara et al., LBL-17705 (1984)

15. TPC Collab., H. Aihara et al., LBL-17616 (1984)

16. J. Dorfan, Proc. of the 1983 Int. Symp. on Lepton and Photon Interactions at High Energy, Ithaca, New York (1983), p. 686

17. C. Bromberg et al., Nucl. Phys. B107, 82 (1976)
T. Kafka et al., Phys. Rev. D16, 1261 (1977)

18. A. Breakstone et al., Phys. Lett. 132B, 458 (1983)

19. G. Arnison et al., Phys. Lett. 132B, 223 (1983)

20. EMC Collab., J.J. Aubert et al., Phys. Lett. 135B, 225 (1984)

21. EMC Collab., J.J. Aubert et al., Phys. Lett. 95B, 306 (1980)

22. G. Schierholz, M. Teper, Z. Phys. C13, 53 (1982)

23. MARK II Collab., J.M. Yelton et al.,
Phys. Rev. Lett. 49, 430 (1982)

24. TASSO Collab., M. Althoff et al., Phys. Lett. 126B, 493 (1983)

25. J.D. Bjorken, Phys. Rev. D17, 171 (1978)
M. Suzuki, Phys. Lett. 71B, 139 (1977)

26. TASSO Collab., R. Brandelik et al.,
Phys. Lett. 117B, 135 (1982)

27. MARK II Collab., M.W. Coles et al., Phys. Rev. D26, 2190 (1982)

28. CLEO Collab., A. Chen et al., Phys. Rev. Lett. 51, 634 (1983)

29. ACCDHW Collab., D. Drijard et al., Nucl. Phys. B155, 269 (1979)

30. TASSO Collab., R. Brandelik et al.,
Phys. Lett. 100B, 357 (1981)

31. CELLO Collab., H.J. Behrend et al.,
Nucl. Phys. B218, 269 (1983), Phys. Lett. 138B, 311 (1984)

32. S. Ellis, Phys. Lett. 117B, 333 (1982)

33. P. Hoyer at al., Nucl. Phys. B161, 349 (1979)

34. A. Ali et al., Phys. Lett. 93B, 155 (1980)

35. JADE Collab., W. Bartel et al., Z.Phys. C21, 37 (1983)

36. TASSO Collab., M. Althoff et al., Z. Phys. C17, 5 (1983)

37. TPC Collab., H. Aihara et al., LBL-17545 (1984)

This report was done with support from the Department of Energy. Any conclusions or opinions expressed in this report represent solely those of the author(s) and not necessarily those of The Regents of the University of California, the Lawrence Berkeley Laboratory or the Department of Energy.

Reference to a company or product name does not imply approval or recommendation of the product by the University of California or the U.S. Department of Energy to the exclusion of others that may be suitable.

TECHNICAL INFORMATION DEPARTMENT
LAWRENCE BERKELEY LABORATORY
UNIVERSITY OF CALIFORNIA
BERKELEY, CALIFORNIA 94720